Limitations in global referencing for robot arms

Sabine HORVATH[1] (ORCID) & Hans NEUNER[1] (ORCID)

[1] TU Wien, sabine.horvath@tuwien.ac.at (corresponding Author)

DOI: 10.3217/978-3-99161-070-0-008, CC BY 4.0

1 Introduction

Robot arms are designed primarily for repetitive tasks such as handling, welding and spraying. Therefore, the most important specification for robot arms is repeatability. However, robot arms also have great potential for other machining tasks, such as drilling, milling and grinding (Wang et al., 2023). These are high-precision robot manufacturing processes which also require absolute pose accuracy. Traditionally, these tasks are performed using CNC machining. Nevertheless, the lower cost, greater flexibility and better adaptability of robot arms make them an attractive alternative. Specific applications of robot machining include drilling in the production of automotive (Ferreras-Higuero et al., 2020) and aerospace (Frommknecht et al., 2017; Diaz Posada et al., 2016) components, as well as milling tasks (Schneider et al., 2015). The main limitations of robot machining identified so far are weak stiffness, instability, and low accuracy in robot arm position (Wang et al., 2023). Schneider et al. (2013) point out that many more applications could be addressed if the accuracy of robot arms were increased. Achieving accuracies in determining the position of a workpiece in the robot frame of approximately 0.1 mm is challenging due to errors accumulating throughout the process, from referencing and imperfections in the robot arm to calibrating tool center points (lever arm) and process-specific deviations (Díaz Posada et al., 2016). This article focuses on referencing and determining the lever arm component. Thus, contributing to the above mentioned challenging aspects of robot machining.

According to Frommknecht et al. (2017), there are three types of referencing: global, semi-local and local. Global referencing requires precise knowledge of the absolute pose of the robot arm and the workpiece in relation to a common coordinate frame. Semi-local referencing also uses a precise global reference, as well as an additional measurement system mounted on the robot arm. Thereby, any discrepancies in the global referencing and in the robot arm positioning are compensated. Local referencing mainly relies on an measurement system mounted on the robot arm. Only a rough global reference is needed. The main difference between the methods is the level of precision of the global reference and whether an internal measurement device is used. This article focuses on global referencing. The position of the robot arm and the workpiece/object must refer to the same reference frame, which is realised by an external measurement device. To achieve this, the object is measured, and the transformation between the measurement coordinate frame and that of the robot arm must be determined. Some literature deals with estimation methods for these parameters (Dornaika and Horaud, 1998, Strobl and Hirzinger, 2006, Tabb and Ahmad Yousef, 2017, Ulrich and Hillemann, 2021). These methods originated in hand-eye calibration (Tsai and Lenz, 1989), where the hand represents the robot arm and the eye corresponds to the camera. Zhuang et al. (1994) extended this method to the simultaneous determination of the robot-world and tool-flange calibration.

Further publications on this topic are Ernst et al. (2012) and Wu et al. (2016). Dornaika and Horaud (1998) were the first to perform a simultaneous robot-world and hand-eye calibration based on a non-linear least squares estimation. However, these approaches do not take stochastic information into account. Ulrich and Hillemann (2021) provide a hand-eye calibration of uncertain robots. They consider data uncertainties in their estimation procedures and additionally estimate the accuracy level of the robot arm poses. The accuracy of global referencing or robot-world transformation depends on the pose accuracy of the robot arm. Due to an insufficiently determined robot arm model, the positional accuracy of robot arms is usually only a few millimeters. In this contribution the simultaneous estimation of the robot-world and tool-flange transformation according to Horvath and Neuner (2019) is used.

This contribution aims to quantify the limitations of the global referencing process and its effects on a machining task. The impact of an insufficiently determined robot arm on the transformation, and consequently on the achievable robot position in the global reference frame is analysed. For this purpose, the transformation poses and the position of the measurement device are varied. These investigations are based on exemplary measurements on a collaborative robot arm.

2 System design

To process a workpiece with a robot arm, the object must be measured by an external measuring device and referenced in the robot arm system by means of a transformation. Consequently, the present system consists of the robot arm, the measuring device, the control system for both, the transformation method and the environment. The important methodical components of this system and the concept for the evaluation are described in the following.

2.1 Robot arm

A robot arm consists of a series of rigid bodies connected by rotary joints. Based on six variable rotary joints θ_i and further constant geometric robot parameters (a_i, α_i, d_i) any pose $\boldsymbol{T}_{RF}^{R}$ can be reached within the robot arm's working area. The robot pose $(\boldsymbol{t}_{RF}^{R}, [\omega, \phi, \kappa])$ is expressed as a homogeneous transformation matrix $\boldsymbol{T}_{RF}^{R}$, consisting of the position $\boldsymbol{t}_{RF}^{R}$ and the orientation $\boldsymbol{R}_{RF}^{R}$. The geometric robot parameters originate from the Denavit-Hartenberg model (Denavit and Hartenberg, 1955). This model concatenates six single transformations $\boldsymbol{T}$ and each transformation is based on four parameters (a, α, d, θ), as indicated in Eq. 1.

$$\begin{bmatrix} \boldsymbol{R}_{RF}^{R} & \boldsymbol{t}_{RF}^{R} \\ \boldsymbol{0} & 1 \end{bmatrix} = \boldsymbol{T}_{1}^{R}\boldsymbol{T}_{2}^{1}\boldsymbol{T}_{3}^{2}\boldsymbol{T}_{4}^{3}\boldsymbol{T}_{5}^{4}\boldsymbol{T}_{RF}^{5} = f(\boldsymbol{a}, \boldsymbol{\alpha}, \boldsymbol{d}, \boldsymbol{\theta}) \tag{1}$$

Insufficiently determined robot parameters result in deviations in the pose of the robot arm. These deviations can be categorised as either geometric or non-geometric. Geometric deviations include all those that can be attributed to insufficiently determined geometric parameters. The latter category includes all time-dependent dynamic influences that change in magnitude during manipulator operation (Schneider et al., 2013). These include joint compliance, gear backlash, gear friction, deflection of the arms, and component heating (Mooring et al., 1991). Additionally, to robot-dependent deviations Schneider et al. (2013)

distinguish between system-dependent and process-dependent deviations. System deviations arise from insufficiently defined robot-dependent parameters, sensor measurement imprecision and deviations in control implementation. Process-dependent deviations are mainly caused by machining forces. The system-dependent deviations are in the focus for further evaluation.

2.2 Transformation

For referencing the robot arm for machining applications (see Sec. 1), two components need to be determined - the reference frame transformation between the measurement device (LT) and the robot arm $\boldsymbol{T}_{LT}^{R}$ as well as the estimation of lever arm components between the end-effector (P) and the robot flange (RF) $\boldsymbol{t}_{RF}^{P}$. A possible approach to this task is treated in Horvath & Neuner (2019) and is used herein. To determine these two transformations, the functional relationship given in Eq. 2 is established. The position of the robot arm $\boldsymbol{t}_{RF}^{R}$ can also be expressed based on the measured pose ($\boldsymbol{t}_{P}^{LT}, [r_x, r_y, r_z]$). Therefore, the lever arm $\boldsymbol{t}_{RF}^{P}$ is added to the measured pose $\boldsymbol{T}_{P}^{LT}$ and then transformed to the robot arm frame $\boldsymbol{T}_{LT}^{R}$. The functional model (Eq. 2) is adjusted in the Gauss-Helmert model. The lower left part in Figure 1 illustrates the transformation chain. The approach formulated in Horvath & Neuner (2019) is built on a measured orientation of the robot arm. If the orientation is not measurable or not available, it is also possible to formulate the functional relation on basis of the robot arm. The robot arm provides orientation information. It is also possible to reach the measured probe position $\boldsymbol{t}_{P}^{LT}$ by adding the lever arm $\boldsymbol{t}_{P}^{RF}$ to the robot pose $\boldsymbol{T}_{RF}^{R}$ and then transform it to the measurement device frame $\boldsymbol{T}_{R}^{LT}$ (Eq. 3).

$$\begin{bmatrix} \boldsymbol{t}_{RF}^{R} \\ 1 \end{bmatrix} = \boldsymbol{T}_{LT}^{R} \cdot \boldsymbol{T}_{P}^{LT} \cdot \begin{bmatrix} \boldsymbol{t}_{RF}^{P} \\ 1 \end{bmatrix} \tag{2}$$

$$\begin{bmatrix} \boldsymbol{t}_{P}^{LT} \\ 1 \end{bmatrix} = \boldsymbol{T}_{R}^{LT} \cdot \boldsymbol{T}_{RF}^{R} \cdot \begin{bmatrix} \boldsymbol{t}_{P}^{RF} \\ 1 \end{bmatrix} \tag{3}$$

The two transformations $\boldsymbol{T}_{LT}^{R}$ (Eq. 2) and $\boldsymbol{T}_{R}^{LT}$ (Eq. 3) are connected by its inverse: $\boldsymbol{T}_{LT}^{R} = \boldsymbol{T}_{R}^{LT^{-1}}$.

2.3 Concept of evaluation

The evaluation of robot referencing is accomplished on the one hand by direct comparison of different transformation results. On the other hand, additional independent measurements are realised by the external measurement device. In Figure 1, a sketch of the evaluation setup is presented. In the left part of the figure, the transformation routine out of Section 2.2 is included. To evaluate these results, additional measurements $\boldsymbol{t}_{P}^{LT,2}$ taken by a second station are required. The transformation between the two laser tracker stations $\boldsymbol{T}_{LT1}^{LT2}$ is established using permanent net point measurements. Equation 4 shows how the evaluation is set up. The net measurements used to derive $\boldsymbol{T}_{LT1}^{LT2}$ are added to the transformation in Eq. 3. This closes the loop, making it possible to compute the deviations $\Delta\boldsymbol{t}_{P}^{LT2}$ from the measured position $\boldsymbol{t}_{P,meas}^{LT2}$.

$$\begin{bmatrix} \Delta\boldsymbol{t}_{P}^{LT2} \\ 1 \end{bmatrix} = \begin{bmatrix} \boldsymbol{t}_{P,meas}^{LT2} \\ 1 \end{bmatrix} - \begin{bmatrix} \boldsymbol{t}_{P}^{LT2} \\ 1 \end{bmatrix} = \begin{bmatrix} \boldsymbol{t}_{P,meas}^{LT2} \\ 1 \end{bmatrix} - \boldsymbol{T}_{LT1}^{LT2} \cdot \boldsymbol{T}_{R}^{LT1} \cdot \boldsymbol{T}_{RF}^{R} \cdot \begin{bmatrix} \boldsymbol{t}_{P}^{RF} \\ 1 \end{bmatrix} \tag{4}$$

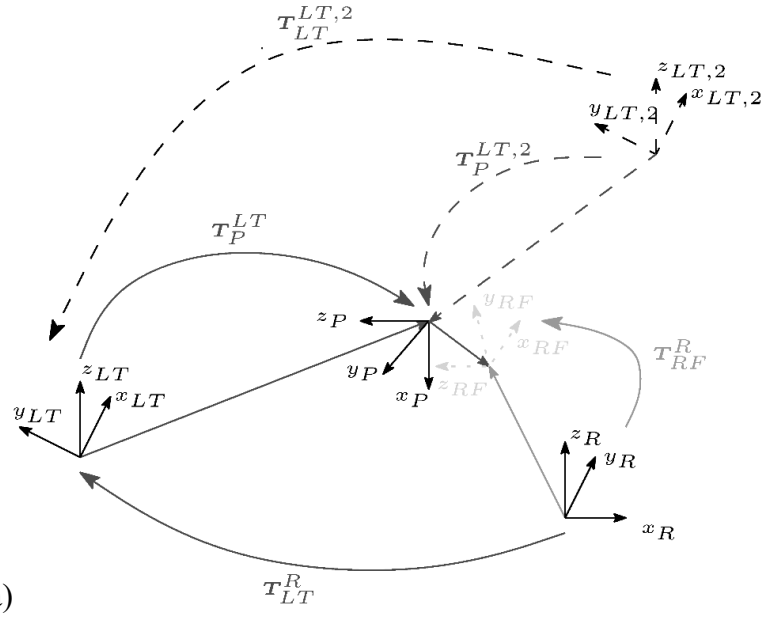

a) b)

Fig. 1: a) Evaluation setup for the referencing of the robot arm. It includes the transformation as defined in Eq. 2 (solid lines) and complements it by an additional measurement station LT2 (dashed lines). b) The robot arm with the T-Probe mounted on the robot flange is shown in the 4D measurement laboratory while measuring with the laser tracker AT960-MR.

3 Evaluation

Before presenting the initial findings, the measurement setup is described, comprising the robot arm, the measuring device and the associated equipment. The first practical step is to test the robot arm on repeatability and accuracy according to ISO 9283. This is followed by the initial referencing results.

3.1 Measurement setup

The measurements are carried out in the 4D measurement laboratory of the Department of Geodesy and Geoinformation at the TU Wien. The laboratory offers stable atmospheric conditions and a highly precise measurement net comprising consoles and ground points with magnetic adapters for 1.5-inch reflectors. The universal robot UR5e is exemplary used for the investigations. Due to its collaborative nature, it does not fulfill the stiffness criteria for robot machining. It is designed for use alongside people and therefore meets different criteria. The external measurement device is a Leica Absolute Tracker AT960-MR. It exhibits an accuracy in position of 0.02 mm (Hexagon, 2021) It is used in combination with 1.5-inch corner cube reflectors (CCR), 1.5-inch super cateye (SCE), which enables ultra-wide acceptance angle of ±75° from vertical around a full 360-degree field of view, and a probing device Leica T-Probe (P), which uses a 0.5 inch tooling ball reflector (TBR). Important specifications are the centering of optics for the various reflector types (<±0.003 mm, <±0.005 mm, <±0.01 mm – CCR, SCE, TBR) and the standard deviations of the ADM constant (±0.003 mm, ±0.005mm, ±0.03mm). The probing device also provides orientation information. The standard deviation

is defined as 0.01°. The corner cube reflector (CCR) is used for the measurements to the net points. The Super Cateye (SCE) is used to measure the position of the robot arm because it enables larger possible incident angles than the CCR (acceptance angle ±30°). The whole robot pose can only be derived by the probing device.

3.2 Robot arm testing

To determine the quality of the UR5e robot arm, we follow the procedure outlined in ISO 9283. We compute the relative pose error or repeatability (RP) and the absolute pose error or accuracy (AP). It is derived for the SCE and the probe. As the ISO 9283 proposes, the robot arm approaches five cube poses 30 times and the laser tracker measures them. By this generated data set, a statistical evaluation is applied and the repeatability is derived. In order to determine the absolute pose error, the transformation between the measurement system and the robot arm must be established. These results are included in Table 3 and will be discussed in detail in the next sections. The results of RP and AP are summarised in Table 1. The table includes the average repeatability in position $\boldsymbol{RP_l}$ and in the three orientation axes $\boldsymbol{RP_a}, \boldsymbol{RP_b}, \boldsymbol{RP_c}$ as well as the accuracy $\boldsymbol{AP}$ averaged over five cube points. Figure 2 provides detailed information about AP in the different coordinate components. The z component is the direction with the least accurate determination. The UR5e's position repeatability according to ISO 9283 amounts to ±25 µm. The manufacturer specifies it as 30 µm. The repeatability in orientation is computed to 0.004°. The orientation standard deviation of the probing device is specified with 0.01°. Consequently, the determined repeatability in orientation cannot be considered statistically proven.

Table 1: Reached average RP and AP by the evaluation of the UR5e according to ISO 9283 (v=10% and 100% and m=600g (SCE)/1.1 kg (Probe)).

	$\overline{RP}_l$	$\overline{RP}_a$	$\overline{RP}_b$	$\overline{RP}_c$	$\overline{AP}_p$
SCE	0.025 mm				0.4 mm
Probe	0.023 mm	0.0044°	0.0031°	0.0038°	0.4 mm

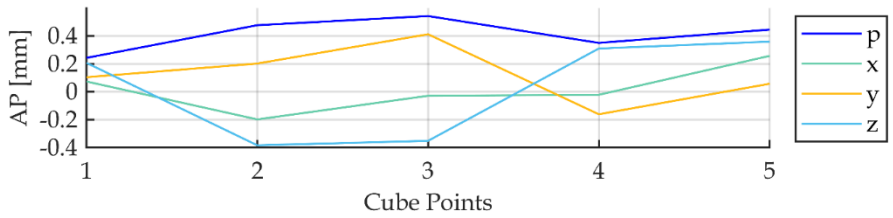

Fig. 2: AP of the UR5e computed on basis of probe measurements. It shows the accuracy (AP) in the single coordinate components (x, y, z) as well as its magnitude (p) for the five cube points.

3.3 Referencing results

This section presents the first results of the global referencing process. The transformations are computed based on the methodology described in Section 2.2. The aim is to demonstrate the effects of different transformations on the absolute positioning of robot arms.

To illustrate a realistic scenario, we begin with two transformation settings that differ considerably. Thus, two different reflectors (SCE/probe), different transformation poses (see Fig. 3), and a different number of poses (17/38 poses) are used. While the SCE data set (Fig. 3, left) has only a few transformation poses with good spatial distribution, the probe data set (Fig. 3, right) offers many poses, mainly on the side aligned with the laser tracker. Compared to the probing device, the SCE does not provide orientation information. Therefore, we use the robot arm's orientation information and compute the transformation chain according to Eq. 3. For comparing the results of Eq. 2 ($\hat{\boldsymbol{x}}_{\boldsymbol{P1}}$) and Eq. 3 ($\hat{\boldsymbol{x}}_{SCE}$), the results of Eq. 3 are inverted ($\hat{\boldsymbol{x}}_{SCE,tr}$), as described in Section 2.2. Table 2 presents the results of the rotational (ω, ϕ, κ) and the translational $(t^R_{LT,x}, t^R_{LT,y}, t^R_{LT,z})$ component of $\boldsymbol{T}^R_{LT}$ and the lever arm components $(t^P_{RF,x}, t^P_{RF,y}, t^P_{RF,z})$.

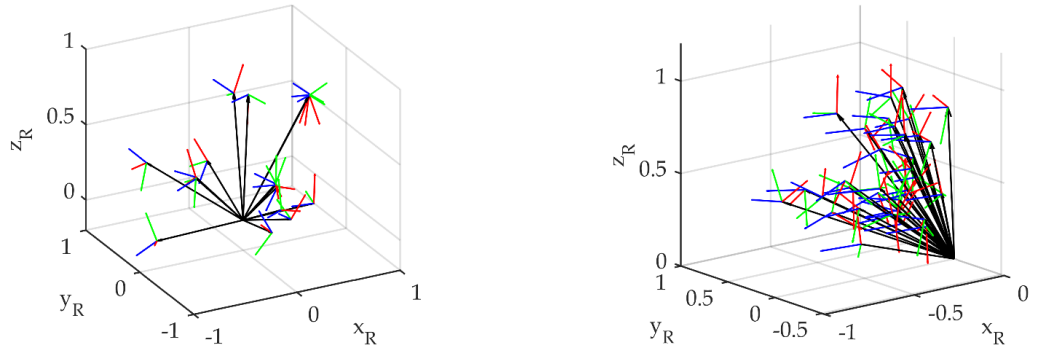

Fig. 3: Transformation poses of the first two data sets – SCE (left), P1 (right). While the SCE data set has few transformation poses with good spatial distribution, the probe data set offers many poses, mainly on the side aligned with the laser tracker.

The transformation parameters determined on basis of the measurements on the super cateye (SCE) are more precise in the translational component ($\hat{\sigma}_{t^R_{LT}}$) despite the small number of transformation poses (17 poses) compared to the measurements to the probe (P1). The rotation component (ω, ϕ, κ) and the lever arm $\boldsymbol{t}^P_{RF}$ are determined more precisely by the probe data set, which is probably due to the large number of poses. Comparing the transformation parameters $\hat{\boldsymbol{x}}_{SCE,tr}$ and $\hat{\boldsymbol{x}}_{P1}$ reveals large differences $\boldsymbol{\Delta}\hat{\boldsymbol{x}}_1$ in the rotation angles ω, ϕ and in $\boldsymbol{t}^R_{LT,z}$, which cannot be explained by the standard deviations of the parameters σ_ω, $\sigma_\phi, \hat{\sigma}_{t^R_{LT,z}}$. The deviation of 0.035° over an average measurement distance of 5 m results in 3 mm, which corresponds to the value of $t^R_{LT,z}$. The derived angle κ differs due to a stationing insufficiency in the software used. The computed lever arms of the SCE and probe are not comparable. The spatial distribution of the points may be one reason for the deviations. It appears that the deviations between the two transformations are mainly caused by the probe data set.

Table 2: Various transformation results belonging to **laser tracker station 1**. One transformation result consists of the parameters $\hat{\boldsymbol{x}}$, the standard deviations $\hat{\boldsymbol{\sigma}}$ as well as deviations $\boldsymbol{\Delta}$ to $\hat{\boldsymbol{x}}_{\boldsymbol{SCE,tr}}$. The dark grey cells are not comparable because of no direct relation. The first two transformations are discussed in Section 3.3, the last two in 4.1.

	$\boldsymbol{\omega}$ [°] [']	$\boldsymbol{\phi}$ [°] [']	$\boldsymbol{\kappa}$ [°] [']	$\boldsymbol{t^R_{LT,x}}$ $[\boldsymbol{m}]$ $[\boldsymbol{mm}]$	$\boldsymbol{t^R_{LT,y}}$ $[\boldsymbol{m}]$ $[\boldsymbol{mm}]$	$\boldsymbol{t^R_{LT,z}}$ $[\boldsymbol{m}]$ $[\boldsymbol{mm}]$	$\boldsymbol{t^P_{RF,x}}$ $[\boldsymbol{mm}]$	$\boldsymbol{t^P_{RF,y}}$ $[\boldsymbol{mm}]$	$\boldsymbol{t^P_{RF,z}}$ $[\boldsymbol{mm}]$
$\hat{\boldsymbol{x}}_{SCE,tr}$	-0.5508	0.4389	37.9550	-5.0764	-0.3488	0.6309	-1.1	65.3	86.9
$\hat{\boldsymbol{x}}_{SCE}$	0.1627	-0.6859	-37.9518	4.2247	-2.8453	-0.5886	1.1	-65.3	86.9
$\hat{\boldsymbol{\sigma}}_{x_{SCE}}$	22	26	21	0.12	0.09	0.06	0.06	0.06	0.12
$\hat{\boldsymbol{x}}_{P1}$	-0.5139	0.4730	234.4406	-5.0764	-0.3481	0.6337	-0.7	-16.2	-113.1
$\hat{\boldsymbol{\sigma}}_{x_{P1}}$	18	18	18	0.09	0.41	0.41	0.03	0.03	0.08
$\Delta\boldsymbol{x}_1$	-0.0369	0.0341		-	0.0007	**-0.0028**			
$\hat{\boldsymbol{x}}_{P2}$	-0.5471	0.4633	234.4483	-5.0761	-0.3488	0.6333	-0.7	-16.1	-113.1
$\hat{\boldsymbol{\sigma}}_{x_{P2}}$	34	38	23	0.29	0.58	0.97	0.09	0.1	0.31
$\Delta\boldsymbol{x}_2$	-0.0037	-0.0244		-0.0003	-	**-0.0024**			
$\hat{\boldsymbol{x}}_{P1b}$	-0.4509	0.3893	234.5386	-5.0754	-0.3563	0.6261	-0.9	-16.3	-113.2
$\hat{\sigma}_{x_{P1b}}$	368	355	388	2.0	8.9	8.3	0.6	0.5	2.1
$\Delta\boldsymbol{x}_{1b}$	**-0.0999**	0.0496		-0.002	**0.0075**	**0.0048**			

For independent control of the derived robot base frame, robot poses are measured from a second laser tracker station, as suggested in Sec. 2.3. The second laser tracker station has been transformed into the first laser tracker station based on measurements to net points offered by the measurement lab. The laser tracker station was chosen quite opposite to the first station. Closing the transformation chain and comparing to the additional measured pose from laser tracker station 2 (Eq. 4), shows the difference vector of [0.1 -0.3 2.6] mm. It corresponds to the differences in the transformation $\Delta\boldsymbol{x}_1$ according to Table 2. The largest difference exhibits in the z-component $t^R_{LT,z}$ by approximately 3mm.

With this example, we demonstrate quite considerable differences between transformations and wish to emphasise the necessity of a well-considered approach to planning the poses and the transformation setup. For this reason, the individual effects will be discussed in the next section.

4 Inference on the global referencing performance

The performance of the referencing depends on the following influences: the number and distribution of poses, the stationing of the measurement device, the reflector type and its mounting. So far, the reflector, the number and distribution of poses are considered in this study. In this section, some of the influences will now be separated in order to better understand their effects.

4.1 Variations in geometry

If a data set of probe observations with a small number of poses but good spatial distribution is available (P2 - Fig. 4, left), the result $\hat{\boldsymbol{x}}_{P2}$ in Table 2 is reached. The data set contains only 9 poses. This increases the standard deviations, especially in the translational z-component $\sigma_{t_{LT,z}^R}$. The deviations change only slightly in most parameters (in comparison to $\Delta\boldsymbol{x}_1$) despite the small number of poses (see Tab. 2). The improved configuration of transformation poses has a strong impact on the discrepances of omega, which decrease by one order of magnitude.

By reducing the data set P1 from 37 poses to 9 poses, the data set P1b is achieved (Fig. 4, right). The aim here is to see the effect of poor spatial distribution in combination with a small number of poses and to compare this with $\hat{\boldsymbol{x}}_{P2}$ (small sample size, but good spatial distribution). The results are also presented in Table 2. They show a poor transformation – the deviations of the translation parameters increase dramatically, especially for the translation components in y- and z-direction, which increase to around 7 and 5 mm respectively. There are two possible reasons for the poor performance of the $\hat{\boldsymbol{x}}_{P1b}$ data set: firstly, the spatial distribution of the poses in the working space of the robot arm (see Fig. 4, right) and secondly, the lower variation in the orientation of the robot pose. These two results ($\hat{\boldsymbol{x}}_{P2}$ and $\hat{\boldsymbol{x}}_{P1b}$) show that the combination of few transformation poses and an insufficient spatial distribution of the poses leads to poor precision and most probably also to poor accuracy of the parameters. The poorer the spatial distribution of the poses in the working space of the robot arm, the more important it is to use more transformation poses.

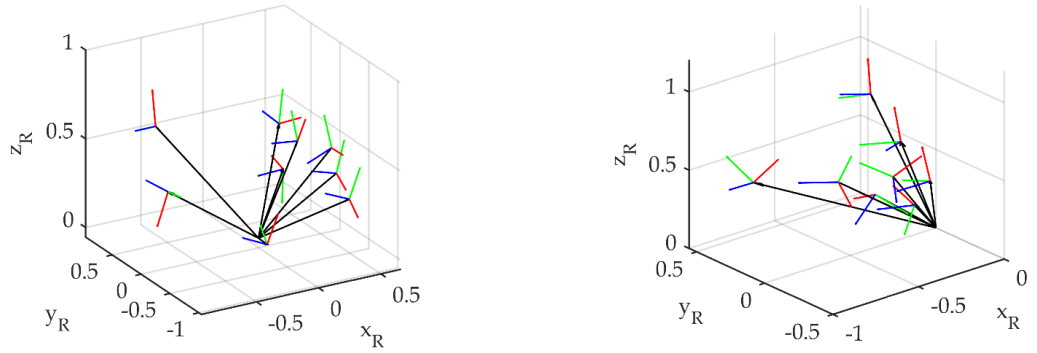

Fig. 4: Transformation poses of one further chosen dataset of probe observations $\hat{\boldsymbol{x}}_{\boldsymbol{P2}}$ and the subsampled one $\hat{\boldsymbol{x}}_{P1b}$ from Table 2 – $\hat{\boldsymbol{x}}_{P2}$ (left), $\hat{\boldsymbol{x}}_{P1b}$ (right). Both exhibit only 9 transformation poses. Clearly, the $\hat{\boldsymbol{x}}_{P2}$ data set has a much better spatial distribution than $\hat{\boldsymbol{x}}_{P1b}$.

4.2 Influence of reflector type

When comparing the standard deviations of the SCE and P1 transformation results (Table 2), despite the additional 20 poses measured, the values for the probe are quite large. To separate the two influences on that, by configuration and by the employed reflector, subsequently a particular focus of the evaluation is set on the reflector type.

Therefore, the same distribution of poses from the P1 data set is measured by the second laser tracker station with SCE and probe. The distribution of the 37 poses is presented in Fig. 3

(right). This builds our third data set and is denoted as e.g. SCE3. To determine the role of the applied model (Eq. 2 or Eq. 3), the probe is treated as reflector (TBR) and the orientation information is neglected. The obtained data set is denoted as P3,TBR. The results of the three different transformations (SCE3; P3; P3,TBR) are included in Table 3.

The smallest standard deviations are achieved by the SCE. Again, the probe with Eq. 2 achieves poorer translational precision $\boldsymbol{\sigma}_{t_{LT}^{R}}$, the rotational standard deviations $\boldsymbol{\sigma}_{\omega,\phi,\kappa}$ are only slightly worse and the lever arm components $\boldsymbol{\sigma}_{t_{RF}^{P}}$ are estimated similarly well. Using only the position measurement to the tooling ball reflector of the probe delivers slightly higher standard deviations for the rotation and the lever arm. However, the translation is estimated much more precise in case of $\hat{\boldsymbol{x}}_{P3,TBR}$ (without considering the measured orientation). In comparison to the SCE results, the less precise manufactured, less accurate determined ADM constant as well as a lower allowable incidence angle may be reasons for the worse performance of the TBR.

Table 3: Various transformation results belonging to **laser tracker station 2**. One transformation result consists of the parameters $\hat{\boldsymbol{x}}$, the standard deviations $\hat{\boldsymbol{\sigma}}$ as well as deviations $\boldsymbol{\Delta}$ to $\hat{\boldsymbol{x}}_{SCE3,tr}$. All three transformations are based on the same pose distribution as presented for P1 measured on laser tracker station 1 (Fig. 3, right). Hence, 37 poses are considered. The dark grey cells are not comparable.

	$\boldsymbol{\omega}$ [°] ['']	$\boldsymbol{\phi}$ [°] ['']	$\boldsymbol{\kappa}$ [°] ['']	$\boldsymbol{t_{LT,x}^{R}}$ $[\boldsymbol{m}]$ $[\boldsymbol{mm}]$	$\boldsymbol{t_{LT,y}^{R}}$ $[\boldsymbol{m}]$ $[\boldsymbol{mm}]$	$\boldsymbol{t_{LT,z}^{R}}$ $[\boldsymbol{m}]$ $[\boldsymbol{mm}]$	$\boldsymbol{t_{RF,x}^{P}}$ $[\boldsymbol{mm}]$	$\boldsymbol{t_{RF,y}^{P}}$ $[\boldsymbol{mm}]$	$\boldsymbol{t_{RF,z}^{P}}$ $[\boldsymbol{mm}]$
$\hat{\boldsymbol{x}}_{SCE3,tr}$	-0.1307	0.1261	30.4662	3.2733	-2.1783	0.6266	-1.4	63.7	-86.9
$\hat{\boldsymbol{x}}_{SCE3}$	0.0487	-0.1750	-30.4660	-1.7150	3.5378	-0.6288	1.4	-63.7	86.9
$\hat{\boldsymbol{\sigma}}_{x_{SCE3}}$	15	15	15	0.06	0.07	0.04	0.02	0.02	0.07
$\hat{\boldsymbol{x}}_{P3}$	-0.1300	0.1271	30.4662	3.2734	-2.1783	0.6265	-0.5	-16.2	-113.1
$\hat{\boldsymbol{\sigma}}_{x_{P3}}$	16	17	17	0.18	0.25	0.29	0.02	0.02	0.07
$\Delta\boldsymbol{x}_3$	0.0007	-0.0010	-	-0.0001	-	0.0001			
$\hat{\boldsymbol{x}}_{P3,TBR}$	0.0520	-0.1743	-30.4617	-1.7150	3.5378	-0.6289	0.0	-16.7	113.0
$\hat{\boldsymbol{\sigma}}_{x_{P3,TBR}}$	19	19	20	0.08	0.09	0.05	0.03	0.03	0.09
$\Delta\boldsymbol{x}_{3,TBR}$	-0.0043	-0.0007	-0.0043	-	-	0.0001			

These effects have not yet been fully clarified. For these investigations, a priori standard deviations of 0.01° are assumed for the robot arm orientation and the probe. The only varying a priori standard deviation is the translational component of the robot arm, which compensates for inconsistencies of the measurement data with respect to the transformation model. For most transformations, the average a priori standard deviation of the robot arm position is approximately 0.18 mm in order to pass the global test of adjustment. Further investigations will include a variance component estimation in order to obtain reasonable results for the orientations as well.

Regarding the influence of the pose distribution discussed in 4.1, one notices for this configuration that only small differences between the estimated transformation parameters

occur for the three cases shown in Table 3. The differences in the translational components reduce from several mm (see Table 2) to few hundredths of mm (see Table 3). Similarly, the differences in the rotational components reduce by two orders of magnitude. Thus, it can be concluded that the high differences between the SCE and probe-based estimations encountered in Table 2 are mainly driven by the extremely different configuration of the measured poses. Beyond the geometric configuration aspect this difference leads also to different influences on the actual pose of the robot arm of non-geometric parameters (see Sec. 2.1).

4.3 Define limitations of global referencing

This section consolidates the results and aims to identify the limitations of global referencing for robot arms. It shows so far, that the greatest influence comes from the pose distribution. As presented in Section 3.3, deviations of up to 3 mm arise between the SCE- and probe-based transformations due to the selected pose distribution (see Table 2). Pursuing this insight further, we created an extended data set with 24 poses (SCE4) which is measured using both, the probe as well as the SCE. This data set should reflect a best case scenario for the global referencing. The distribution of the poses is given in Figure 5. The obtained results for the best-case transformation (Tab. 4) confirm the conclusions of the previous sections: using the SCE instead of the probe leads to lower standard deviations of the estimated transformation parameters (see also Sec. 4.2, $\hat{\boldsymbol{\sigma}}_{x_{SCE3}}$ vs. $\hat{\boldsymbol{\sigma}}_{x_{P3}}$). This applies especially to the translation. When observing the same poses with both reflector types the estimated parameters are almost similar with discrepancies $\Delta\boldsymbol{x}_3$ for the translational components in the range of one tenths of a mm. Also the discrepancies $\Delta\boldsymbol{x}_3$ and $\Delta\boldsymbol{x}_4$ behave similarly. The results are presented in Table 4 and relate to Table 3 due to the same laser tracker station. Comparing the translation results $\hat{\boldsymbol{x}}_{SCE3,tr}$ (Table 3) and $\hat{\boldsymbol{x}}_{SCE4,tr}$ (Table 4), results in a deviation of 1.7 mm. Opposing this deviation ($\Delta\boldsymbol{x}_{3,4}$, Table 4) with $\Delta\boldsymbol{x}_1$ in Table 2, a decrease of the discrepancies can be noted. Thus, by increasing the number of transformation poses, the deviations between independent transformation results decrease. Further measurements and investigations are required to prove the limit of the discrepancies in global referencing, which will be probably limited by the accuracy of the robot arm.

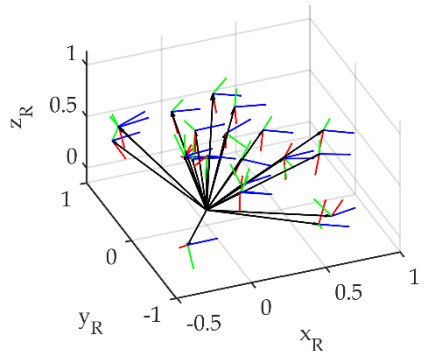

Fig. 5: Transformation poses for the SCE4 and P4 transformation. It bases on the pose distribution of data set SCE (Fig. 3, 16 Poses) and is extended by 8 poses.

All investigations so far have been accomplished for one specific collaborative robot arm and need to be derived for different ones. While the aforementioned magnitudes of the results will not apply to other robot arms, this is likely to be true with regard to the classification of influences according to their importance.

Table 4: Transformation results of spatial well distributed poses belonging to **laser tracker station 2**. One transformation result consists of the parameters $\hat{\boldsymbol{x}}$, the standard deviations $\hat{\boldsymbol{\sigma}}$ as well as deviations $\boldsymbol{\Delta}$ to $\hat{\boldsymbol{x}}_{SCE4,tr}$. The transformations are based on the extended data set of SCE (Fig. 5). Hence, 24 poses are considered. The dark grey cells are not comparable. $\Delta \boldsymbol{x}_{3,4}$ relates to $\hat{\boldsymbol{x}}_{SCE3,tr}$ out of Table 3.

	$\boldsymbol{\omega}$ [°] [']	$\boldsymbol{\phi}$ [°] [']	$\boldsymbol{\kappa}$ [°] [']	$\boldsymbol{t}^{R}_{LT,x}$ $[\boldsymbol{m}]$ $[\boldsymbol{mm}]$	$\boldsymbol{t}^{R}_{LT,y}$ $[\boldsymbol{m}]$ $[\boldsymbol{mm}]$	$\boldsymbol{t}^{R}_{LT,z}$ $[\boldsymbol{m}]$ $[\boldsymbol{mm}]$	$\boldsymbol{t}^{P}_{RF,x}$ $[\boldsymbol{mm}]$	$\boldsymbol{t}^{P}_{RF,y}$ $[\boldsymbol{mm}]$	$\boldsymbol{t}^{P}_{RF,z}$ $[\boldsymbol{mm}]$
$\hat{\boldsymbol{x}}_{SCE4,tr}$	-0.1071	0.1464	30.4783	3.2737	-2.1776	0.6251	-1.4	63.5	-86.9
$\hat{\boldsymbol{x}}_{SCE4}$	0.1348	0.1214	-30.4785	-1.8358	-3.4761	-0.6294	1.4	-63.5	86.9
$\hat{\boldsymbol{\sigma}}_{x_{SCE4}}$	18	18	15	0.07	0.11	0.05	0.05	0.05	0.12
$\hat{\boldsymbol{x}}_{P4}$	-0.1078	0.1456	30.4790	3.2736	-2.1776	0.6251	-0.1	-16.0	-112.8
$\hat{\boldsymbol{\sigma}}_{x_{P4}}$	19	21	17	0.21	0.26	0.35	0.05	0.05	0.14
$\Delta \boldsymbol{x}_4$	0.0007	0.0008	-0.0007	0.0001	-	-			
$\Delta \boldsymbol{x}_{3,4}$	-0.0236	-0.0203	-0.0121	-0.0004	-0.0007	**0.0015**			

The biggest limitation in global referencing for robot arms is the distribution of the transformation poses. As shown in Table 2 (P2 vs P1), nearly nine well-distributed poses determined by probe measurements deliver the same result as 37 poorly distributed poses. This demonstrates the importance of geometry. A sufficient number of transformation poses ranges between 17 to 24. This depends on the distribution of poses and on the reflector type. Starting with 15 poses achieves a precision of up to 0.1 mm for a robot arm with positional accuracy of 0.4 mm, ensuring good spatial distribution and a super cat eye reflector. Due to the larger standard deviations reached by probe measurements (see Tab. 3), more poses are needed to achieve a precision of 0.1 mm for the translational parameter.

Applying these investigations to another (type) robot arm will demonstrate how dependent the transformation results are on the accuracy of the robot arm. For the used UR5e, we derived an average positional accuracy expressed as deviation from the nominal position of 0.4 mm according to ISO 9283 (see Tab. 1). During the adjustment process to estimate the transformation parameters, the a priori standard deviation in the position of the robot arm is in average 0.2 mm. Passing the global test indicates that chosen functional and stochastic models are in accordance with the data set. As the deviations obtained from the ISO lie within the 2-sigma interval of the standard deviation resulting from the adjustment, the two results are consistent, and it is feasible to claim a standard deviation of the robot arm of 0.2 mm. To calculate the standard deviation based on a defined procedure and in accordance with all measurement types, the variance component estimation proposed in Section 4.2 can be used. The standard deviation for the transformation parameters lies in the same order of magnitude.

However, the deviation between independent transformation sets ranges from 3 to1.5 mm. There is still a fairly large difference, which we need to take into account. This can be mainly attributed to influences due to the geometric distribution of the poses as well as systematic deviations of the robot arm coming from both geometric and non-geometric components.

5 Conclusion and outlook

Accurate referencing of workpieces to robot arms enables robot manufacturing processes such as drilling, milling and grinding. This article deals with quantifying the influences on determining transformation parameters through global referencing using laser tracker measurements. The influences discussed in detail are the distribution and number of poses, and the reflector type. The distribution of the poses was identified as the most limiting influence. It was found that the Super Cateye performs better than the probe, achieving lower standard deviations, particularly when translating the laser tracker frame to the robot arm frame. An appropriate number of poses is between 17 and 24. This depends on the pose distribution, reflector type, and targeted precision. Future research will investigate the differences in transformation performance when using the probe or the SCE, subsequently focusing on the SCE. Variance component estimation can contribute to our understanding of these differences. Additionally, it can be beneficial for adequately quantifying the precision of the robot arm.

Literature

DENAVIT, J., & HARTENBERG, R. S. (1955): A Kinematic Notation for Lower-Pair Mechanisms Based on Matrices. Journal of Applied Mechanics 22, No. 2, p.215–21. https://doi.org/10.1115/1.4011045.

TSAI, R.Y., & LENZ, R.K. (1989): A New Technique for Fully Autonomous and Efficient 3D Robotics Hand/Eye Calibration. IEEE Transactions on Robotics and Automation 5, No. 3, p. 345–58. https://doi.org/10.1109/70.34770.

ISO 9283 (1998): Manipulating industrial robots — Performance criteria and related test methods. International Organization for Standardization

DORNAIKA, F., & HORAUD, R. (1998): Simultaneous Robot-World and Hand-Eye Calibration. IEEE Transactions on Robotics and Automation 14, No. 4, p.617–22. https://doi.org/10.1109/70.704233.

MOORING, B., ZVI ROTH, & DRIELS, M. (1991): Fundamentals of Manipulator Calibration. John Wiley & Sons

ZHUANG, H., ROTH, Z.S. & SUDHAKAR, R. (1994): Simultaneous Robot/World and Tool/Flange Calibration by Solving Homogeneous Transformation Equations of the Form AX=YB. IEEE Transactions on Robotics and Automation 10, No. 4, p.549–54. https://doi.org/10.1109/70.313105.

STROBL, K., & HIRZINGER, G. (2006): Optimal Hand-Eye Calibration. 2006 IEEE/RSJ International Conference on Intelligent Robots and Systems, 4647–53. https://doi.org/10.1109/IROS.2006.282250.

ERNST, F., RICHTER, L. MATTHÄUS L., MARTENS, V., BRUDER, R. SCHLAEFER, A. & SCHWEIKARD, A. (2012): Non-orthogonal Tool/Flange and Robot/World Calibration. The International Journal of Medical Robotics and Computer Assisted Surgery 8, No. 4, p.407–20. https://doi.org/10.1002/rcs.1427.

SCHNEIDER, U., POSADA, J.R.D., & VERL, A. (2015): Automatic Pose Optimization for Robotic Processes. 2015 IEEE International Conference on Robotics and Automation (ICRA), 2054–59. https://doi.org/10.1109/ICRA.2015.7139468.

SCHNEIDER, U., DRUST, M. & ANSALONI, M., LEHMANN, C., PELLICCIARI, M., LEALI, F., GUNNINK, J.W. & VERL A. (2016): Improving Robotic Machining Accuracy through Experimental Error Investigation and Modular Compensation. The International Journal of Advanced Manufacturing Technology 85, No. 1–4, p.3–15. https://doi.org/10.1007/s00170-014-6021-2.

WU, L., WANG, J., KEYU WU, L.Q., REN, H. & MENG, M.Q.-H. (2016): Simultaneous Hand–Eye, Tool–Flange, and Robot–Robot Calibration for Comanipulation by Solving the AXB=YCZ Problem. IEEE Transactions on Robotics 32, No. 2, p.413–28. https://doi.org/10.1109/TRO.2016.2530079.

DIAZ POSADA, J. R., SCHNEIDER, U., PIDAN, S., GERAVAND, M., STELZER, P., & VERL., A. (2016): High Accurate Robotic Drilling with External Sensor and Compliance Model-Based Compensation. IEEE International Conference on Robotics and Automation (ICRA), 3901–7. https://doi.org/10.1109/ICRA.2016.7487579.

TABB, A., UND KHALIL M., & YOUSEF, A., (2017): Solving the Robot-World Hand-Eye(s) Calibration Problem with Iterative Methods. Machine Vision and Applications 28, No. 5–6, 569–90. https://doi.org/10.1007/s00138-017-0841-7.

FROMMKNECHT, A., KUEHNLE, J., EFFENBERGER, I., & PIDAN, S. (2017): Multi-Sensor Measurement System for Robotic Drilling. Robotics and Computer-Integrated Manufacturing 47, 4–10. https://doi.org/10.1016/j.rcim.2017.01.002.

HORVATH, S., & NEUNER, H, (2019): System Identification of a Robot Arm with Extended Kalman Filter and Artificial Neural Networks. Journal of Applied Geodesy 13, No. 2, p.135–50. https://doi.org/10.1515/jag-2018-0045.

FERRERAS-HIGUERO, E., LEAL-MUÑOZ, E., GARCÍA DE JALÓN, J., CHACÓN, E. & VIZÁN, A. (2020): Robot-Process Precision Modelling for the Improvement of Productivity in Flexible Manufacturing Cells. Robotics and Computer-Integrated Manufacturing 65, 101966. https://doi.org/10.1016/j.rcim.2020.101966.

HEXAGON MANUFACTURING INTELLIGENCE (2021): Absolute Tracker systems and accessories, Vs. 2.0

ULRICH, M., & HILLEMANN, M. (2021): Generic Hand–Eye Calibration of Uncertain Robots. 2021 IEEE International Conference on Robotics and Automation (ICRA), 11060–66. https://doi.org/10.1109/ICRA48506.2021.9560823.

WANG, W., GUO, Q., YANG, Z., JIANG, Y. & XU, J. (2023): A State-of-the-Art Review on Robotic Milling of Complex Parts with High Efficiency and Precision. Robotics and Computer-Integrated Manufacturing 79, 102436. https://doi.org/10.1016/j.rcim.2022.102436.